Chapter 11

Nonlinear Femtosecond Optical Spectroscopy Techniques in Photosynthesis

Donatas Zigmantas, Ying-Zhong Ma, Elizabeth L. Read and Graham R. Fleming*
Department of Chemistry, University of California, Berkeley, Physical Biosciences Division, Lawrence Berkeley National Laboratory, B77 Hildebrand Hall, Berkeley, CA 94720, U.S.A

Summary

Over the past ten years, the techniques and sophistication of analysis of ultrafast spectroscopy have advanced to a remarkable extent. Following the demonstration and validation of new methods using simple dilute dye solutions, many applications of these new techniques have been to photosynthetic systems. The reasons for this are not hard to find: photosynthetic pigment protein complexes function through a delicate interplay of interpigment and pigment-environment interactions, and standard methods provide an unsatisfactory level of microscopic insight because signals are dominated by inhomogeneous effects, or the methods themselves are insensitive to the interactions between states of interest. The developments described in this chapter are designed to address all these issues. Multiphoton transient absorption spectroscopy helps to unravel complex energy transfer and relaxation pathways. Two-photon excitation spectroscopy prepares states that are not ac-

*Author for correspondence, email: GRFleming@lbl.gov

Thijs J. Aartsma and Jörg Matysik (eds): Biophysical Techniques in Photosynthesis II, pp. 201–222.

cessible directly from the ground state. Photon echo methods defeat inhomogeneous broadening, measure it, and exploit it to observe energy transfer between chemically identical donors and acceptors. Two-dimensional techniques explicitly reveal electronic couplings and the pathways of energy flow. New methods based on Raman spectroscopy reveal vibrational frequencies in excited states, and indeed a wide range of transient species.

I. Introduction

The technology of generating and characterizing tunable, intense, ultrashort light pulses has matured, and experimentalists have now turned to using these pulses to provide more incisive and detailed probes of photosynthetic systems. For example, the system can be subjected to more than one excitation pulse prior to the probing event. The transfer of population between potential energy surfaces at a series of different times can be very useful in disentangling complex relaxation pathways. The electric field strength of pulses tens of femtoseconds in duration is necessarily high, permitting observation of nonlinear processes such as two-photon absorption. This allows direct population of states whose optical transition from the ground state is forbidden in one-photon absorption, such as the lowest excited singlet states of polyenes and in particular carotenoids in photosynthetic light-harvesting. Photon echo based methods, in particular the peak shift and two-dimensional Fourier transform electronic spectroscopy, provide new insights into the design principles of light-harvesting pigment-protein complexes. The peak shift method enables defeat of, quantification of, and use of the inhomogeneous energy level distribution of the ensemble of chromophores to reveal energy transfer over a very broad range of timescales. The newly developed two-color peak shift technique has potential to reveal electronic couplings, wavefunction overlaps, and pathways of energy flow. Perhaps the technique with the greatest potential to reveal the microscopic design principles of natural light-harvesting is the method of two-dimensional Fourier transform photon echo spectroscopy. This technique, analogous to two-dimensional NMR methods, reveals electronic couplings between individual molecules directly. A series of such spectra, recorded at different time intervals after the initial pulse, map out the relaxation pathways in time and (implicitly) in space. This has already led to new insights into the mechanism of energy flow within the Fenna-Matthews-Olson (FMO) complex of green sulfur bacteria, and seems likely to produce real advances in our understanding of light-harvesting in plant and bacterial systems.

Electronic spectroscopy of large molecules such as chlorophyll in condensed phase environments do not provide any information on the vibrational spectra of transient species, which can be crucial to determining the electronic structure and molecular geometry of the molecule. Newly developed methods in visible pump-infrared probe (covered in Chapter 10, Groot and van Grondelle) and two-dimensional infrared spectroscopy and stimulated Raman spectroscopy combine both high time resolution with high spectral resolution to provide detailed insight into the nuclear motions involved in the relaxation processes, thereby offering an important complement to the spectroscopy of electronic states.

In this chapter, we describe all of these new techniques and illustrate them with examples of application to photosynthetic systems.

Abbreviations: (B)Chl – (bacterio)chlorophyll; 2C3PEPS – two-color three pulse photon echo peak shift; 2D – two-dimensional; 3PEPS – three pulse photon echo peak shift; Car – carotenoid; ESA – excited state absorption; FMO – Fenna-Matthews-Olson; FROG – frequency-resolved optical gating; fs – femtosecond; FSRS – femtosecond stimulated Raman spectroscopy; FWHM – full-width half-maximum; ICT – intramolecular charge transfer; IVR – intramolecular vibrational relaxation; LH1 – primary light-harvesting complex; LH2 – peripheral light-harvesting complex; LHC II – light-harvesting complex II; LO – local oscillator; MP-TA – multipulse transient absorption; NOPA – noncollinear optical parametric amplifier; OPA – optical parametric amplifier; PAP – pump-action-probe; PDP – pump-dump-probe; PEPS – photon echo peak shift; PP – pump-probe; PrPP – pump-repump-probe; SPIDER – spectral phase interferometry for direct electric-field reconstitution; TP – two-photon; TPE – two-photon fluorescence excitation

II. Developments in Laser Technology and Pulse Measurement Techniques

Recent years have seen remarkable progress in solid state ultrafast laser technology. Since the invention of the self-mode-locked Ti:Sapphire laser in 1990 (Spence et al., 1991), the field has evolved very rapidly: now 10–20 fs pulses are produced routinely

(Asaki et al., 1993) and 5-fs pulses can be generated directly from Ti:Sapphire oscillators using specially designed chirped mirrors to compensate for dispersion introduced by the Ti:Sapphire crystal in the cavity (Morgner et al., 1999; Kartner et al., 2004). Pulses with a few to under two optical cycles can also be generated from amplified or cavity-dumped low-repetition Ti:Sapphire lasers systems employing different pulse compression techniques (Baltuska et al., 1997; Nisoli et al., 1997; De Silvestri et al., 2004). There is also a range of optical parametric amplifiers able to generate sub-10 fs pulses at all possible wavelengths in the visible and near-IR regions. For example, the noncollinear optical parametric amplifier (NOPA) (Wilhelm et al., 1997; Butkus et al., 2004) is widely used in a variety of ultrafast spectroscopy experiments. Significant advances have been made not only in laser technology, but also in the field of ultrashort pulse characterization. Interferometric techniques like frequency-resolved optical gating (FROG) (Trebino et al., 1997) and spectral phase interferometry for direct electric-field reconstitution (SPIDER) (Iaconis and Walmsley, 1999) deliver a full characterization of pulses in electric field and phase. Fully computerized tunable laser systems with full pulse characterization are commercially available. Fiber lasers (Fermann et al., 1997) and supercontinuum generation in microstructure optical fibers (Ranka et al., 2000) are among the most promising developments towards low power and substantially less expensive lasers systems. This array of high performance laser systems and pulse characterization techniques has enabled a variety of new time-resolved spectroscopic methods with unprecedented time resolution, sensitivity and flexibility.

III. Multipulse Transient Absorption Spectroscopy

A. Technique

Multipulse transient absorption (MP-TA) assumes various forms such as pump-dump-probe (PDP) (Gai et al., 1997; Larsen et al., 2003) stimulated emission pumping (Kovalenko et al., 1998; Ruhman et al., 2002), two-pump and probe (Logunov et al., 2001), and pump-repump-probe (PrPP) (Larsen et al., 2003). This class of techniques involves using an additional pulse in the standard pump-probe (PP) scheme. In MP-TA experiment, an intense pump pulse produces a nonequilibrium population of excited states whose evolution is perturbed with a variably delayed, intense action pulse, resulting in partial depletion of the population in a particular state or states. The pump-induced differential absorption (ΔOD) of a sample and its change arising from the interaction of the action pulse is monitored by a weak probe pulse at either a selected wavelength or over a broad spectral range. Data acquisition usually involves measuring the ΔOD signals in the presence (pump-action-probe (PAP)) and in the absence (PP) of the action pulse by varying the time delay between the pump and probe pulses (t) while keeping the delay between the pump and action pulses (τ) fixed. Occasionally, measurements of ΔOD signals as a function of τ for a fixed t may be also performed, enabling direct access to the temporal dependence of the ΔOD changes caused by the action pulse (Larsen et al., 2003). A successive detection of the $\Delta ODPAP$ and $\Delta ODPP$ signals at each time delay, t or τ, is preferable to ensure identical experimental conditions. This detection can be readily realized by introduction of a mechanical shutter into the action beam, or by simultaneous modulation of the pump and the action beams with, for instance, two optical choppers operating at different frequencies (Larsen et al., 2004). In the latter case, the signal induced by the action pulse, $\Delta ODAP$, should also be measured, especially when this pulse is spectrally resonant with the ground state absorption of the sample.

The most convenient way to differentiate the ΔOD change caused by the action pulse is to subtract the PP signal, $\Delta ODPP$, from the $\Delta ODPAP$ signal, and the result is usually defined by a double difference absorption signal (Larsen et al., 2004; Papagiannakis et al., 2004):

$$\Delta\Delta OD(\lambda,t,\tau) = \Delta OD_{PAP}(\lambda,t,\tau) - \Delta OD_{PP}(\lambda,t) \qquad (1)$$

where λ denotes the probe wavelength. In addition, the $\Delta ODAP$ signal should also be subtracted when the action beam is modulated. From Eq. (1), it is clear that the $\Delta\Delta OD$ signal is opposite in sign to the PP signal, i.e., it has a negative sign for ESA but a positive sign for bleaching and stimulated emission (Kovalenko et al., 1998; Larsen et al., 2004).

A successful application of the MP-TA technique relies largely on proper selection of the frequency of the action pulse. An exclusive or preferential selection of a well-characterized excited-state by tuning the frequency of the action pulse can usually greatly simplify data analysis. For a chosen excited

state, different frequencies of the action pulse can be used to match a transition to a final state with either higher or lower energy. However, a criterion should be fulfilled in selecting the final state: the relaxation to the perturbed state must proceed slowly enough to allow time resolution of the Δ*OD* change induced by the action pulse. Furthermore, successive perturbation of different excited states by varying the frequency of the action pulse is often needed for a complex system (Larsen et al., 2003).

B. Applications

Applications of the MP-TA technique to condensed phase systems have demonstrated its capability for unraveling overlapping spectral features (Kovalenko et al., 1998; Larsen et al., 2003) and for disentangling complex pathways of excited state relaxation (Gai et al., 1997; Logunov et al., 2001; Ruhman et al., 2002; Papagiannakis et al., 2004). Until now, the application of this technique to photosynthesis has been focused on identifying new electronic states of carotenoids (Cars) in solution. Larsen and coworkers performed the MP-TA experiment on a hexane solution of β-carotene (Larsen et al., 2003). After excitation of its S2 state at 400 nm, an 800 nm pulse was applied to preferentially repump the population from the S1 state to a higher excited-state. The resulting −ΔΔOD spectrum characterizing the ESA spectrum of the Car S_1 state is markedly different from the PP data obtained at the same time delay *t*, indicating that the latter contains contributions from additional state(s). In another experiment, after excitation at 400 nm a 530 nm pulse, spectrally resonant with both the S_2 emission and the S_1 ESA bands, was applied to simultaneously dump the population of the S_2 state to the ground state and to repump the S_1 state. Target analysis of the data enabled the authors to ascribe the observed feature to a new electronic state, $S^{\ddagger}$ (Fig. 1).

The second application concerns peridinin, a carbonyl Car with spectral properties depending strongly on the polarity of the environment. A change of solvent from nonpolar to polar gives rise to markedly different spectra and lifetimes, which was attributed to stabilization of an intramolecular charge transfer (ICT) state in the polar medium. To gain a better understanding about the relation between the S_1 and the ICT state, Papagiannakis and coworkers performed PDP measurements on a methanol solution of peridinin (Papagiannakis et al., 2004). In this experiment, peridinin was excited at 530 nm, an 800 nm dump pulse was applied to preferentially transfer population from the ICT state to ground state, and the induced change was monitored by a broadband probe pulse. The kinetics measured at different probe wavelengths clearly show that the dump pulse selectively interacts with the ICT state but not the S_1 state, and this observed difference demonstrates that the S_1 and the ICT states are distinct (Fig. 2). Target analysis of the experimental data further enabled the

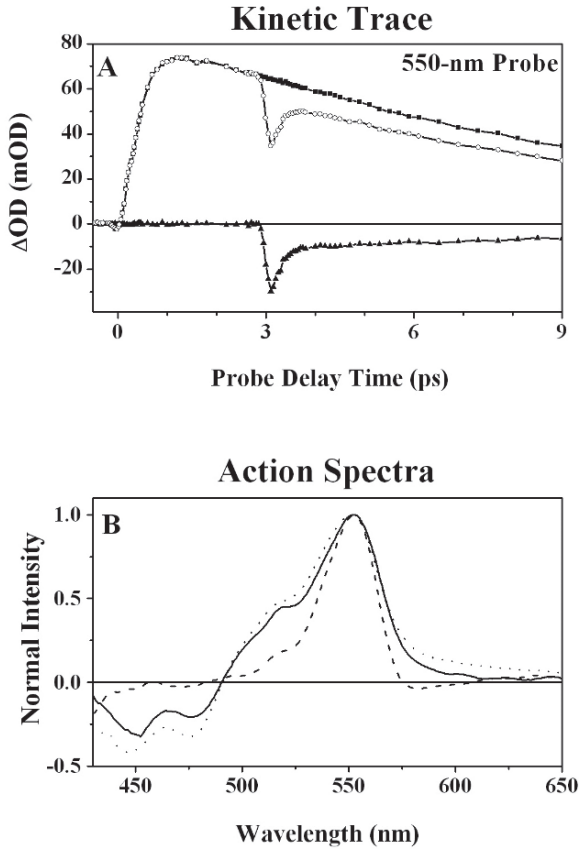

Fig. 1. (a) TA kinetics of β-carotene in hexane measured upon pumping at 400 and probing at 550 nm in the absence (filled squares) and in the presence (open circles) of a 530 nm pulse applied at 3 ps with respect to the pump pulse. The resulting ΔΔOD profile (filled triangles) is shown at the bottom of the panel. (b) Comparison of the 3 ps pump-probe spectrum (dotted line) with the spectra obtained from a target analysis of the ΔΔOD data collected at different probe wavelength as a function of τ, the delay between the first two pulses. The probe delay was set to $t = 3$ ps. The data analysis resulted in two spectra, inverted by multiplying by (–1), with lifetimes of ~300 fs and ~10 ps, characterizing the S_2 dumping (solid line) and the S_1 repumping (dashed line), respectively. All three spectra were normalized at the maximum (Larsen et al., 2003). (Fig. courtesy of D.S. Larsen, Univ. of California, Davis)

authors to propose a network of complex relaxation pathways involving S_1, S_2, ICT, and a ground state intermediate.

Future applications of this technique to photosynthetic systems, in which the pigments are electronically coupled, are expected to further advance our understanding of the energy transfer pathways, especially those difficult to assess by conventional PP and fluorescence upconversion techniques. However, special care should be taken in these applications. First, the overall intensity of the pump and the action pulses should be kept at a level that is well below the initiation threshold of non-linear dynamic processes, e.g., singlet-singlet and singlet-triplet excitation annihilation (van Amerongen et al., 2000). Occurrence of these processes and their concomitant changes of spectral shapes caused, for instance, by a local heating (Valkunas and Gulbinas, 1997) will complicate data analysis, and in certain cases may even prohibit extracting useful information from the experimental data. Second, prolonged illumination of a sample by two intense laser pulses may cause permanent degradation; therefore, independent experiments must be conducted in order to assess the integrity of the sample.

IV. Two-Photon Fluorescence Excitation and Pump-Probe Spectroscopy

Two-photon (TP) absorption involves an electronic transition from an initial to a final state by simultaneous absorption of two quanta of electromagnetic radiation. When the final state fluoresces or undergoes relaxation by transferring energy to a fluorescent acceptor, highly sensitive detection of TP absorption can be achieved by the two-photon fluorescence excitation (TPE) technique. Since a TP transition follows selection rules that are different from those of a one-photon process, the TPE serves as a sensitive tool for probing excited states that cannot be directly reached by one-photon excitation.

Over the past four decades, TP absorption has become an important tool in the field of molecular spectroscopy. For an in-depth description of the theory, experimental techniques, and various early applications, we refer to the monographs and reviews by McClain (1974), McClain and Harris (1977), Friedrich and McClain (1980), Birge (1983), Shen (1984), and the references therein. In this section, we will focus on the techniques of TPE and TP-excited

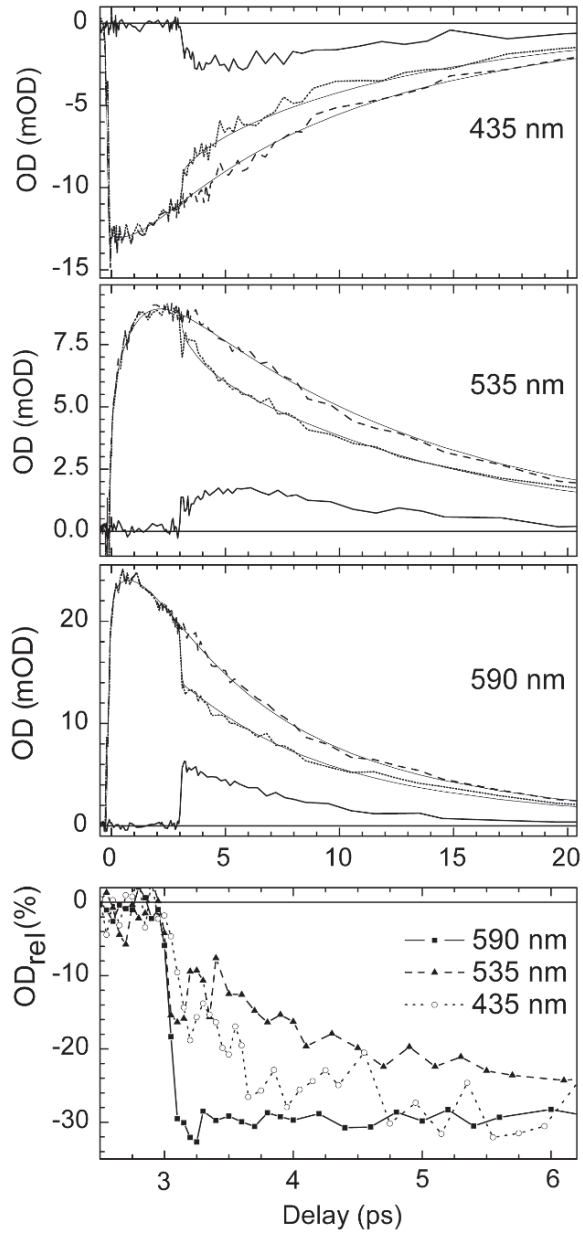

Fig. 2. Pump-probe (dashed lines) and pump-dump-probe (dotted lines) kinetic traces of peridinin in methanol measured at 435, 535 and 590 nm, monitoring the population evolution in the ground state, S_1 and ICT state, respectively. The thin solid lines through the data denote the target analysis fit, while the thick solid lines correspond to the depletion ($-\Delta\Delta OD$) signal. The lowest panel shows the relative loss signals ($\Delta\Delta OD_{rel}$) at 435, 535 and 590 nm, which is defined by $\Delta\Delta OD_{rel} = \Delta\Delta OD(\lambda,t,\tau)/\Delta OD(\lambda,t)$. From the $-\Delta\Delta OD$ and $\Delta\Delta OD_{rel}$ signals, it is clear that the interaction of a 800 nm dump pulse at 3 ps results in an instantaneous population depletion from the ICT state (590 nm curve), whereas the responses of the S_1 (535 nm curve) and S_0 (435 nm curve) states to this perturbation are significantly slower (Papagiannakis et al., 2004). (Fig. courtesy of R. van Grondelle, Vrije Universiteit, Amsterdam)

pump-probe (PP) that are based on femtosecond (fs) laser excitation, and their latest applications to photosynthetic systems.

A. Femtosecond Two-Photon Fluorescence Excitation Spectrophotometer

The basic setup of a single beam fs TPE spectrophotometer consists of a tunable fs laser source for exciting a sample, a reference detector and a signal detector for monitoring the intensities of the two-photon excitation light and its induced fluorescence emission, respectively, and an auto-correlator for measuring continuously the temporal length of the laser pulses. Because TPE is a second-order process in interaction with the electric field, the experimentally measured fluorescence intensity at a chosen frequency ω_1, $F(\omega_1)$, is proportional to the square of the incident power of the excitation pulse tuned to ω_2, $P(\omega_2)$. When the variation of pulsewidth at different wavelengths is negligible, a TPE spectrum can be readily obtained by measuring $F(\omega_1)/p_2(\omega_2)$ at different values of ω_2. Complications arise when the pulsewidth is not constant in the spectral range of interest, and because of its dramatic effect on the emission intensity, a proper correction is necessary in order to obtain a correct TPE spectrum. For pulses with simple analytical temporal profiles, such as Gaussian or hyperbolic secant squared ($sech^2$), the pulse width effect can be corrected by simply multiplying $F(\omega_1)/p_2(\omega_2)$ with the corresponding pulse full-width half-maximum (FWHM), $\tau(\omega_2)$. When the pulse shape is not of a simple analytical form, correction of this pulse width effect can be done numerically.

A schematic diagram of an experimental set up for TPE experiments in our laboratory is shown in Fig. 3 (Zimmermann et al., 2002). Because the cross section of TP absorption is many orders of magnitude smaller than that of the typical one-photon absorption (Fischer et al., 1995; Xu and Webb, 1996), and the quantum yield of fluorescence emission is often small, detection of fluorescence emission upon TP excitation usually requires a tight focus of the excitation beam in combination with efficient emission collection.

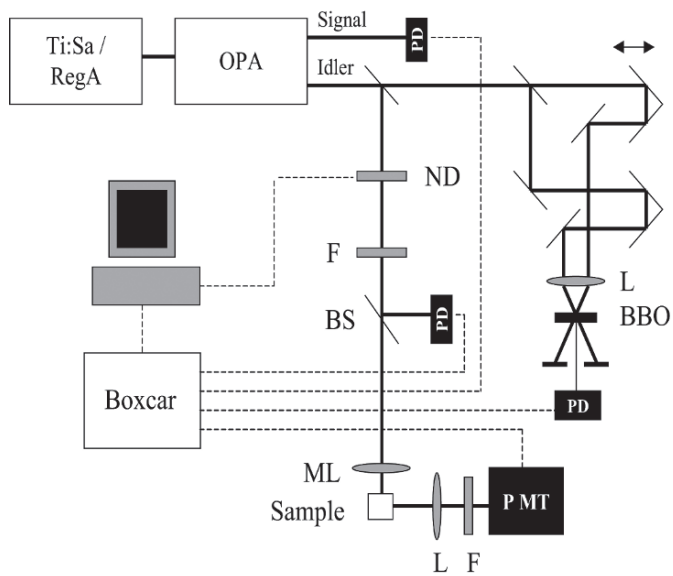

Fig. 3. Schematic diagram of a single beam TPE spectrophotometer. The excitation source is a 2 kHz Ti:Sapphire regenerative amplifier pumped OPA, and its idler output provides near-infrared pulses tunable from 900 to 1600 nm, with a typical pulse energy of 20 nJ and a temporal width of 95 fs. A beam splitter (BS) is used to separate a small portion of the excitation light for monitoring the excitation intensity with a calibrated photodiode (PD). The majority of the excitation light is focused to the sample with a microscope objective (Nikon E10, N.A. 0.25, focal length: 6 mm), denoted by ML. The emitted fluorescence light is collected at 90 degrees by a 5 cm lens (L) and focused onto a photomultiplier (PMT). The outputs of the detectors were preamplified and measured by two boxcar integrators (Stanford Research SR250), synchronized using the signal output of the OPA. A neutral density filter wheel (ND) is used to continuously vary the intensity of excitation light, and emission wavelength was selected using a bandpass filter (F). Before each experiment the excitation beam is sent into an autocorrelator, which was used to measure the pulsewidth and to determine the spectral shape of the pulse by doubling it in the autocorrelator BBO crystal (Zimmermann et al., 2002).

Gated or lock-in detection must be utilized in order to effectively suppress any stray light. Furthermore, when high energy pulses are used, care should be exercised to ensure that the tightly focused beam does not generate a white-light continuum from the walls of the cuvette and/or the sample solution, which can cause direct one-photon excitation of the sample and produce much more intense emission.

Measurement of a TPE spectrum involves the following steps: (1) tuning the wavelength of the OPA; (2) determining the pulse width; (3) measuring the power dependence of the TPE fluorescence, fitting the data with a second-order polynomial, and determining the amplitude of the second-order term (which provides a quantitative measure of the relative two-photon absorption intensity); (4) correcting the effect of pulse width, if necessary, and finally (5) constructing the TPE spectrum. In addition to the TPE spectrum measurements, time-resolved TPE experiments can be performed by employing the fluorescence upconversion technique.

B. Two-Photon Excitation Pump-Probe

While conceptually identical to the conventional PP technique based on one-photon excitation (Jimenez and Fleming, 1996), several essential prerequisites must be met in setting up a successful TP-excitation-based PP experiment. The first prerequisite is to generate a detectable concentration of excited molecules, especially when the pulse energy for TP excitation is low, e.g., on the order of 10 nJ or less. Possible ways to do this include (1) tightly focusing the pump beam with a lens or objective with a short focal length, thereby increasing the photon density in the excitation volume; (2) using a concentrated sample for efficiently capturing available photons. The collinear geometry for the pump and probe beams enables detection of all molecules in the excitation volume, and an enhancement of the detected signal with a signal-to-noise ratio comparable to that observed in the PP data upon one-photon excitation has been demonstrated (Linden et al., 2004).

The second prerequisite is to choose a suitable test sample for finding the PP signal and optimizing the sensitivity of the set-up. Inexpensive choices include commonly used organic solvents, e.g., acetone, ethanol, methanol, etc., and a criterion for selecting a particular solvent is that its transmission cut-off wavelength (Lide, 1996) must be equal to or longer than the wavelength corresponding to the energy of three-photon absorption, i.e., two photons from the pump pulse and one photon from the probe pulse. This solvent response is instantaneous, with a temporal profile similar to the cross-correlation function of the pump and probe pulses, and therefore a time step of a fraction of the pulse width should be used to scan the delay between the pump and probe pulses. A properly selected solvent is capable of producing a very large signal, which, for sub-100 fs pump pulses, is approximately two orders of magnitude larger than the signal from Cars dissolved in organic solvents or bound in pigment-protein complexes. The extremely low signal from molecules under study, on the other hand, requires high-sensitivity detection such as lock-in amplification and effective noise suppression, in order to obtain high-quality data. A simple noise suppression method involves simultaneous monitoring of the intensity fluctuations of the pump and probe pulses with separate detectors, and normalizing the PP data.

Verification that the detected signal truly arises from TP excitation becomes crucial when additional, unwanted electronic states, such as the triplet state of (bacterio)chlorophyll ((B)Chl) or the S_2 state of certain Cars, can contribute. In addition to quadratic dependence on the excitation power (McClain and Harris, 1977), the ratio of the signals obtained by circularly versus linearly polarized excitation serves as an additional mark of a TP process (Birge and Zhang, 1990). Since it depends on the symmetries of the molecule's excited- and ground-state wave functions (McClain, 1971), knowledge about this ratio must be available from either theoretical calculations or independent measurements on the given molecule or one that is structurally similar to it.

C. Applications

A significant application of the TPE technique to photosynthesis involves the verification of the involvement of the Car S_1 state in energy transfer processes to Chl or BChl molecules. Indirect evidence for such an involvement has been found by comparing the S_1 lifetimes of Cars in solution and in light-harvesting (LH) complexes, and by resolving the rise times of the relevant energy acceptor Chl or BChl molecules (Polivka and Sundström, 2004). Because these experiments are performed by exciting directly the Car S_2 state, interpretation of the collected data is often complicated by multiple potential energy transfer pathways such as Car

S_2 to (B)Chl and between (B)Chls, as well as possible contributions from vibrational relaxation within the acceptor molecules. A further complication, albeit less significant than the complication arising from the S_2 state, is due to the dependence of the S_1 lifetime on the solvent (Macpherson et al., 2001), which results in considerable difficulty of defining a 'standard' lifetime for comparison with the in situ lifetime of the same Car. Selective excitation of a Car S_1 state with TP absorption in combination with detection of its acceptor fluorescence greatly simplifies this verification. Krueger and coworkers have measured the TPE spectrum of spheroidene (Fig. 4), the principal Car in the LH2 of purple bacterium *Rhodobacter* (*Rb.*) *sphaeroides* (Krueger et al., 1999). By directly exciting its S_1 transition with TP absorption, observation of the fluorescence emission from the BChls enabled the authors to verify unambiguously for the first time the involvement of the Car S_1 state in the Cars $\rightarrow$ BChls energy transfer process. Furthermore, a detailed analysis of the TPE spectral band shape allowed an estimate of 13 900 $\pm$150 cm^{-1} to be made for the $S_0 \rightarrow S_1$ transition energy.

Direct TP excitation of the Car S_1 state with fs pulses allows observation of subsequent dynamics with a probe pulse tuned to its $S_1 \rightarrow S_n$ transition. Thus, interference arising from other excited states of the Car can be eliminated. Walla and coworkers have performed PP measurements on three LH complexes of purple bacteria using a probe pulse centered at 550 nm (Walla et al., 2000). The experimental data can be satisfactorily described by a mono-exponential decay plus a constant offset. An example of the kinetic decays measured upon TP excitation at 1310 nm is shown in Fig. 5a. The TP nature of the experimentally measured signals was verified by a quadratic intensity dependence of the amplitude associated with the exponential decay (Fig. 5b), and a change of the BChl fluorescence emission intensity with the polarization of the excitation beam (linear vs. circular) (Fig. 5d). In addition, the linear power dependence of the offset signal (Fig. 5c) indicated a distinct one-photon origin of this signal. In another experiment the TPE spectrum of LHC II, the major light-harvesting complex of Photosystem II in green plants, was determined by Walla, et al. (Walla et al., 2000). Also, the time dependence of Chl fluorescence after TPE measured by fluorescence upconversion showed a very fast (~250 fs) Chl fluorescence rise, corresponding to the energy transfer from the Car S_1 state to the Chls.

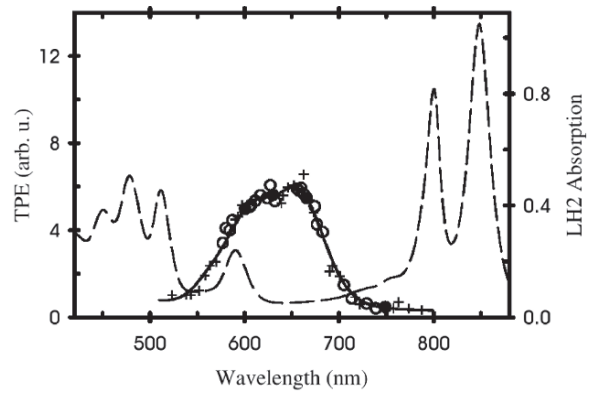

Fig. 4. The TPE results obtained for the LH2 of *Rb. sphaeroides*. The experiments were performed using a 250 kHz Ti:Sapphire regenerative amplifier pumped OPA in combination with lock-in detection. The TPE data (symbols) and fit (solid line) are shown on a wavelength scale together with the one-photon absorption spectrum (dashed line). The TPE data were obtained from three independent measurements, and the points from individual datasets are given by pluses. In combining three separate datasets in a single TPE spectrum, points averaged from all three datasets are shown with filled circles, while points averaged from two datasets are shown with open circles (Krueger et al., 1999, with permission).

Currently, measurement of the TPE spectrum of Car S_1 state is restricted to those Cars with S_2 states that are well separated from S_1 or strictly TP forbidden. When an S_2 state is accessible by TP absorption and the energies of the S_1 and S_2 states are similar as observed for peridinin, the resulting TPE spectrum contains limited information about the S_1 state (Zimmermann et al., 2002; Shima et al., 2003). However, most Cars are nonpolar molecules and do not carry a static dipole moment in the S_2 state and therefore their S_2 state is TP forbidden by the symmetry. On the other hand, TP-excited PP has so far been limited to detection of kinetics at the selected probe wavelength. Frequency-resolved measurements, particularly in the spectral region of energy acceptor absorption, await future explorations.

V. Three Pulse Photon Echo Peak Shift Spectroscopy

A. Principles of Photon Echo Spectroscopy

If the dynamical processes contributing to the broadening of a spectral line can be separated into very rapid (homogeneous) and ultraslow (inhomogeneous) contributions on the experimental timescale and if

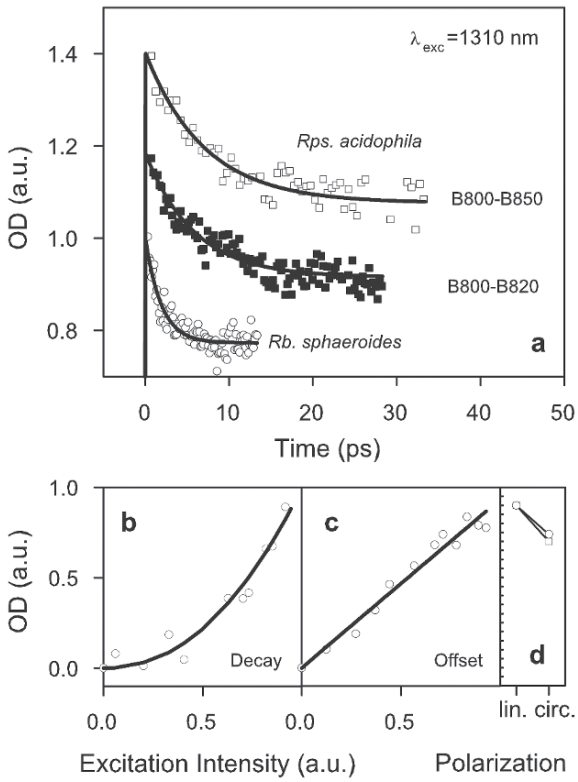

Fig. 5. Time dependence of ESA signals detected at 550 nm for different LH complexes of purple bacteria: (□) B800-B850 and (■) B800-B820 from *Rps. acidophila* and (○) LH2 from *Rb. sphaeroides*, and the solid lines show the corresponding mono-exponential fits with lifetimes of 7 ± 0.5, 6 ± 0.5 and 1.9 ± 0.5 ps, respectively. The traces were vertically offset for clarity. The pump and probe beams were generated using a 250 kHz Ti:Sapphire regenerative amplifier pumped OPA, arranged in a non-collinear geometry. (b) Power dependence of the amplitude associated with the mono-exponential fit of the data of *Rb. sphaer*oides, and the solid line shows the fit by an exponent of 2.2 ± 0.3. (c) Linear power dependence of the constant offset obtained from the fit to the data of *Rb. sphaeroides*. (d) Relative intensity of the fluorescence measured after TPE at 1310 nm with linear and circular polarized light of LH2 from *Rps. acidophila* (□) and *Rb. sphaeroides* (○), with a corresponding ratio of 0.80 ± 0.04 and 0.84 ± 0.04, respectively (Walla et al., 2000).

the inhomogeneous broadening is very large, (as is the case in nuclear magnetic resonance experiments), then simply measuring the decay of the intensity of the photon echo signal can provide valuable information on the homogeneous (T_2) timescale of the system (Aartsma et al., 1996). Early attempts to use ultrashort pulses in a photon echo experiment on a condensed phase system were made on this notion. However, condensed phase systems in general, and photosynthetic systems in particular, have a continuous range of timescales associated with them and do not have effectively infinite inhomogeneous broadening, so meaningful information cannot be obtained in this way. A decade ago Cho and Fleming and coworkers found that a different quantity, the three photon echo peak shift (PEPS) is directly related to the solvation dynamics of dye molecules in solution (Cho et al., 1996). Related work was also carried out by Wiersma and co-workers (deBoeij et al., 1996). The one-color PEPS (using three pulses (3PEPS)) was extended to the study of population transfer and incoherent energy transfer (Yang and Fleming, 1999a; Yang et al., 1999), and to more strongly coupled systems where coherent effects play a role (Yang and Fleming, 2000; Ohta et al., 2001). Yang and Fleming proposed a two-color version of the peak shift for the study of electronic coupling in dimers (Yang and Fleming, 1999b) and the method was experimentally demonstrated (Agarwal et al., 2002a; Prall et al., 2004). Cho and Fleming explored the application of one- and two-color peak shifts to coupled chromophore systems and provided a comparison with the two-dimensional photon echo spectroscopy (Cho and Fleming, 2005) described in Section VI of this chapter.

B. One-Color Three Pulse Photon Echo Peak Shift Spectroscopy

Three pulse stimulated photon echoes are generated by focusing a series of three identical, variably delayed, ultrashort laser pulses onto a sample (for a detailed description of the experiment, see Joo et al., 1996). In the perturbative (weak-field) limit, the effect of the laser field on the sample can be thought of as follows. The first pulse prepares the system in a coherent superposition state, and after a time delay τ (the coherence time), the second pulse transfers the system to a population state. Then, after waiting a time T (the population time), the third pulse returns the system to a coherent state. The reader new to this field may wonder how the effects of the 3 pulses can be differentiated in this manner — this is done by the experimental geometry which utilizes interference (or equivalently momentum conservation) to enforce the sequence of events just described for a signal detected in a specific direction, $\mathbf{k}_S = -\mathbf{k}_1 + \mathbf{k}_2 + \mathbf{k}_3$, where the various $\mathbf{k}$'s are the wavevectors of the signal (S) and pulses 1–3, respectively. This ability to separate signals spatially is a unique advantage of optical spectroscopy over NMR. In a disordered sample, rephasing can occur during the second coherence

period to reverse the effect of dephasing during the first coherence period, and in this case a macroscopic polarization, marked by emission of a photon echo, is generated in the sample. Dynamics in the system ranging from a few femtoseconds to hundreds of picoseconds are tracked by varying the population time. In a 3PEPS measurement, the time-integrated photon echo signal is collected for a fixed population time as the coherence delay is scanned. The peak shift is considered to be the coherence delay at which the maximum echo signal is recorded. The fact that integration is performed over the final time period, *t* (Fig. 6), (as well as over the frequency range of the signal in general) makes the 3PEPS technique particularly simple to apply, as it does not require interferometric stability in the optical delays or complex signal processing to extract the required data.

The peak shift is a useful parameter because it is essentially a measure of the time correlation function of the electronic transition frequencies in an ensemble. This memory function, *M*(t) (Yan and Mukamel, 1990), is given by:

$$M(t) = \frac{\langle \delta\omega(t)\delta\omega(0) \rangle}{\langle \delta\omega^2(0) \rangle} \tag{2}$$

where $\delta\omega(t)$ describes the fluctuations of the electronic transition frequency of each chromophore and the angular brackets represent ensemble averages. The transition frequency as a function of time of the *i*th chromophore is given by:

$$\omega_i(t) = \delta\omega(t) + \langle\omega\rangle + \varepsilon_i \tag{3}$$

where ε_i is the energetic offset in the inhomogeneous distribution and $\langle\omega\rangle$ is the average electronic transition frequency. The transition frequency is affected by interactions with the solvent, intramolecular vibrations, and energy transfer processes. Simultaneous fitting of the linear absorption spectrum and peak shift decay with a model *M*(t) therefore yields a wealth of information about system dynamics. In particular, the initial peak shift value is a measure of

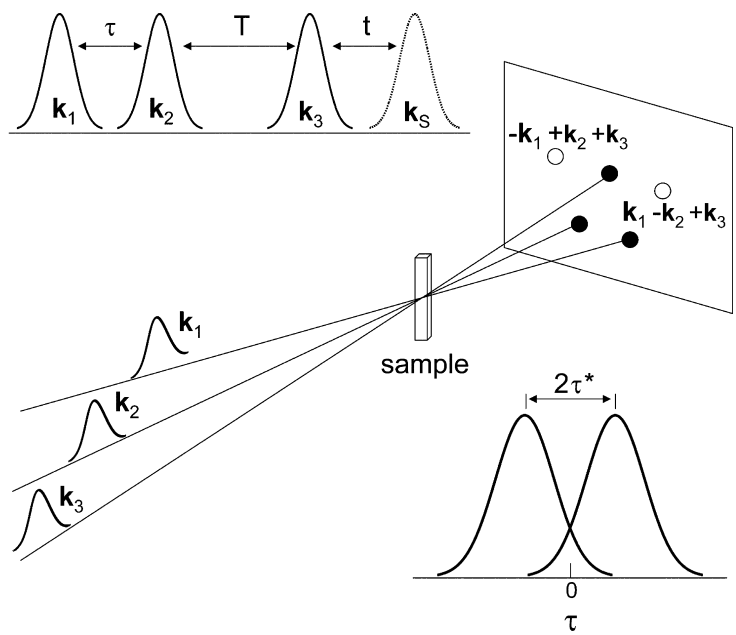

Fig. 6. Pulse sequence, phase matching, and peak shift for the three-pulse photon echo. The three pulses, incident on the sample with wave vectors $\mathbf{k}_1$, $\mathbf{k}_2$, and $\mathbf{k}_3$, generate two mirror-image echo signals in the phase matched directions $\mathbf{k}_1-\mathbf{k}_2+\mathbf{k}_3$ and $-\mathbf{k}_1+\mathbf{k}_2+\mathbf{k}_3$, as indicated in the diagram by the open circles. The experimentally controllable time delays between the first and second pulses and between the second and third pulses are the coherence time (τ) and population time (*T*), respectively. After waiting time t following interaction with the third pulse, the photon echo signal is emitted. The lower diagram is a schematic of the integrated photon echo signal intensity versus coherence delay. The peak shift (τ*) is defined as the coherence delay at which the echo signal is maximum, or, more precisely, half the difference between the corresponding signals collected in both phase matched directions.

the system's coupling to the environment, long-time values are indicative of disorder in the system that is static on the timescale of the experiment, and the decay profile contains information about dynamical processes. It has been demonstrated that the peak shift is particularly sensitive to energy transfer processes inside the laser bandwidth, and relatively insensitive to inter-band transfer processes that remove population from the pulse window (Yang and Fleming, 1999a). The reason for this insensitivity is that in a dilute system with inhomogeneous broadening the peak shift does not decay to zero at very large values of population time, T, because the excitation is unable to 'average' over the entire distribution of energy gaps. With energy transfer the situation changes: now the excitation can visit a representative collection of sites and the peak shift will decay to zero with a timescale set by the energy transfer timescale.

A key experimental condition of 3PEPS is that all transitions of interest must lie within the laser pulse bandwidth. Two-color 3PEPS, in which the third pulse is a different color from the first two, has been developed in recent years to circumvent this requirement. The one-color experiment utilizes a three beam interferometer, where the equal-intensity beams are split from the same fs laser source, and two beams are intercepted by computer-controlled delay stages. Lock-in processing is done to minimize scatter, and phase-matching conditions can be exploited to separate the photon echo signal from other signals and background. When the three input beams are arranged noncollinearly in an equilateral triangle geometry (from a head-on view), the photon echoes are emitted from the sample in phase-matched directions $\mathbf{k}_1 - \mathbf{k}_2 + \mathbf{k}_3$ and $-\mathbf{k}_1 + \mathbf{k}_2 + \mathbf{k}_3$ (see Fig. 6). These signals contain identical information and are mirror images of each other. Both are collected, and half the distance between them is taken as a precise measure of the peak shift.

3PEPS experiments on photosynthetic light-harvesting complexes reveal interactions among pigments and between pigments and the membrane proteins that surround them. Jimenez, et al., showed that the initial peak shift values (~25 fs) for primary light-harvesting complex (LH1) and LH2 of purple photosynthetic bacteria are higher than observed for typical laser dyes in polar solvents, indicating weak coupling of the complexes to their protein-solvent surroundings (Jimenez et al., 1997). This weak coupling may be a key aspect of efficient light-harvesting, because dissipation of energy to the surroundings during the 50 ps transfer time from LH2 to LH1 to the reaction center is minimized. That the rapid (~150 fs) decay in the peak shift for the detergent isolated LH1 complex is due to energy transfer around the ring is nicely demonstrated in Fig. 7 in which the peak shift decay of an intact LH1 ring is compared with the peak shift decay for the B820 subunit of LH1 which contains just two BChl molecules (Yu et al., 1997). The solid lines represent two calculations with identical input parameters except that the energy transfer rate is set to zero for the B820 sample. The large long-time peak shift value for the B820 subunit, both observed and predicted, results from the inhomogeneous broadening, which is averaged over by energy transfer in the 28 BChl LH1 complex. Direct observation of specific energy transfer processes through peak shift measurements was also demonstrated clearly by Agarwal and coworkers in a 3PEPS study comparing isolated LH2 complexes with complexes in native membranes (Agarwal et al., 2002b). The isolated sample was detergent-solubilized so that the inter-complex distance was large, while the membrane sample, prepared from a mutant strain that contained only LH2, mimicked the wild-type membrane where LH2 rings come into close contact and energy can transfer between them. The results of the peak shift measurement using 850 nm excitation are shown in Fig. 8. The samples show similar initial decay timescales of 100–200 fs, but the membrane sample shows an additional decay component of ~5 ps. The ultrafast initial decay is ascribed to intra-complex exciton relaxation, while

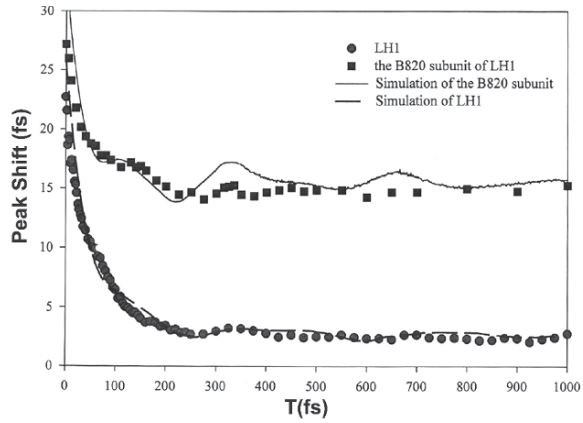

Fig. 7. 3PEPS measurements of LH1 of *Rb. sphaeroides* (circles) and the B820 subunit from LH1 of *Rhodospirillum (Rs.) rubrum* (squares). The solid lines represent two simulations with identical input parameters except that the energy transfer rate is set to zero for the B820 sample (Yu et al., 1997, with permission).

the 5 ps component is attributed to inter-complex (LH2-LH2) energy transfer in the membrane. Additionally, the difference between these two peak shift traces demonstrates that the static disorder of LH2 apparent in the linear spectrum is a combination of intra- and inter-complex disorder (Yang et al., 2001). That is, there are two distributions of energies corresponding to the energies of BChls within individual rings and the energies of the LH2 complexes in the membrane. Energy transfer within the ring destroys the memory of intra-complex disorder, just as energy transfer through the membrane destroys the memory of inter-complex disorder. The presence of the long 5 ps decay in the membrane sample indicates the timescale of LH2-LH2 energy transfer, as well as confirming that two levels of energetic disorder are present in the photosynthetic complexes.

C. Two-Color Three Pulse Photon Echo Peak Shift Spectroscopy

In Two-color three-pulse photon echo peak shift (2C3PEPS) spectroscopy, the first two pulses have the same spectrum ('color') and the third pulse has a different, non-overlapping spectrum ('color'). Clearly, two versions of the method are possible — 'downhill' in which the second color is of longer wavelength then the first and the 'uphill' in which the reverse applies. At first sight the method seems an almost trivial extension of one-color 3PEPS, but the technique turns out to be a complementary method to 2D photon echo spectroscopy, providing information on the spatial overlap of electronic states, mixing coefficients between coupled chromophores, and remarkably, pathway-dependent information on the spectral evolution of a dynamical system.

A particularly interesting use of one- and two-color 3PEPS lies in the ratio of the one-and two-color peak shifts $\tau^*(T)$ as a function of population time, T (Yang and Fleming, 1999b)

$$\frac{\tau^*_{ONE}(T)}{\tau^*_{ONE}(T)+\tau^*_{TWO}(T)} = 2\left\{1-\frac{2A_C(T)}{A_1(T)}\right\}\cos^2\theta\sin^2\theta \qquad (4)$$

where θ is the mixing angle,

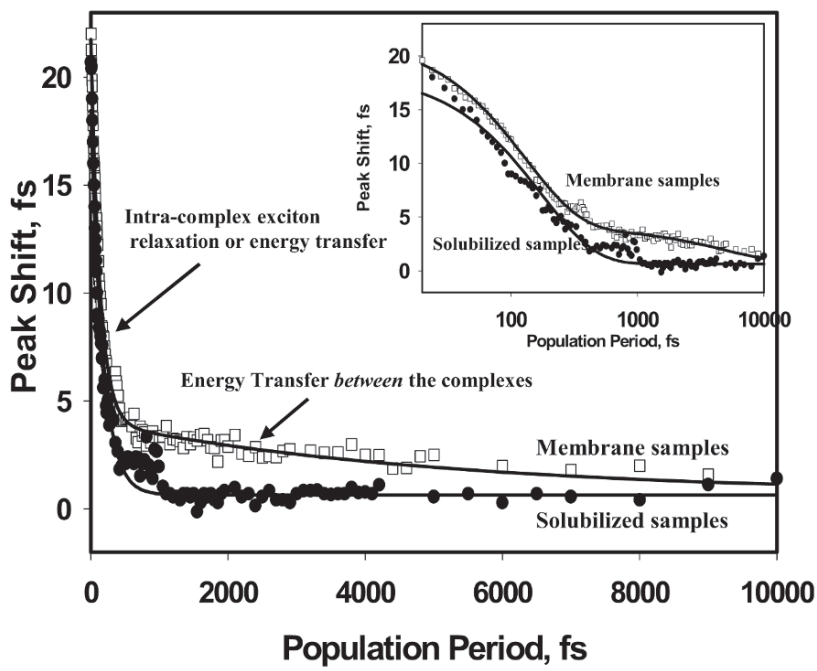

Fig. 8. 3PEPS data for the B850 band of LH2 from *Rb. sphaeroides* at room temperature. The circles and squares correspond to the detergent solubilized samples and native membrane samples, respectively. The membrane samples are obtained from a mutant strain containing LH2 as the sole BChl-protein complex. The inset shows the same data on a logarithmic scale. The solid lines represent exponential fits to the data. The data for the solubilized samples are best described by a single-exponential decay component (95%, 160 fs), whereas the membrane samples are best fit by two exponential components (80%, 180 fs, 16%, 5 ps) (Agarwal et al., 2002b, with permission).

$$\theta = \frac{1}{2}\arctan\left(\frac{2J}{\varepsilon_1 - \varepsilon_2}\right) \quad (5)$$

with J the coupling and ε_1 and ε_2 the monomer site energies. $A_1(t)$ is the real part of site energy fluctuation correlation function, the un-normalized form of $M(t)$ and $A_c(t)$ is the identical quantity describing the fluctuations in J. Thus for a homodimer, by measuring both one-color 3PEPS and 2C3PEPS and calculating the ratio in Eq. (4) as a function of T, one can estimate (1) the mixing angle, (2) the coupling constant, J and (3) the ratio of $A_c(T)/A_1(t)$. This approach has been used by (Prall et al., 2004) to successfully extract the coupling constant for a phthalocyanine dimer system.

The two-color peak shift method is still under active development and the reader is referred to couple of references (Cho and Fleming, 2005; Prall et al., 2005) for the most recent ideas.

VI. Femtosecond Two-Dimensional Fourier Transform Electronic Spectroscopy

A. Principles of Two-Dimensional Spectroscopy

At the end of the nineties, multidimensional femtosecond spectroscopy emerged as a powerful new tool to study ultrafast dynamics, interactions and transient structures of complex molecular systems. This new technique was inspired by the tremendous success of multidimensional Fourier transform magnetic resonance spectroscopy, e.g., in structure determination of large molecules and magnetic resonance imaging. Advances in ultrafast lasers (see Section II) have allowed the adoption of many two-dimensional (2D) techniques from magnetic resonance for applications in infrared and optical spectroscopy. The basic concept of two-dimensional spectroscopy is as follows. The behavior of the spectrum is probed across a range of single excitation frequencies, yielding two dimensions of frequency information and thus revealing connections between molecular transitions corresponding to specific frequencies. More complex 2D techniques use spectral interferometry and Fourier transform (FT) tools to obtain full amplitude and phase information of the system polarization. The measured electric field is separated into its real and imaginary parts, conveying information about the absorption (real part) and refractive properties (imaginary part) of the system under investigation. The real part can be interpreted as the transient field amplitude at probe frequency ω_t (the detection frequency) due to excitation at frequency ω_τ (the coherence frequency) after waiting time T (the population time). The imaginary part describes transient changes in the refractive index in an analogous way. The time resolution is defined by the length of the excitation pulses, and frequency resolution is limited only by the detection system and uncertainty principle set by the resonances in the sample itself, rather than the laser pulses. Pioneering 2D experiments for vibrational transitions were performed using dynamic hole burning (Hamm et al., 1998) and heterodyne-detected photon echoes (Asplund et al., 2000; Hochstrasser et al., 2000; Golonzka et al., 2001). 2D Fourier transform spectroscopy in the visible-domain is closely related to its infrared-domain counterpart, although the technique is somewhat more difficult. 2D Fourier transform electronic spectroscopy (we will use '2D electronic spectroscopy' from now on) is complicated by difficult-to-achieve phase stability at shorter, visible wavelengths and generally broad electronic transitions resulting in the overlap of various peaks in the 2D spectra. 2D spectroscopy for electronic transitions was introduced and discussed in detail in a series of excellent publications by Jonas and coworkers (Hybl et al., 1998; Faeder and Jonas, 1999; Jonas, 2003). Foundations for the theoretical explorations of vibrational and electronic 2D spectroscopy were laid by Mukamel (1995, 2000).

2D electronic spectroscopy is especially well suited for studies of multi-chromophoric protein complexes in photosynthesis because it probes electronic couplings between chromophore molecules and explores the distribution of instantaneous molecular environments and geometries.

B. Experiment and Analysis

The technique of 2D electronic spectroscopy discussed here is based on measuring three pulse photon echoes, which are described in detail in section V of this chapter. The goal of 2D electronic spectroscopy is to obtain the complete third-order optical response function of investigated systems, which can include molecular aggregates or any excitonically coupled system. In contrast to the 3PEPS experiment, heterodyne detection of the photon echo are required

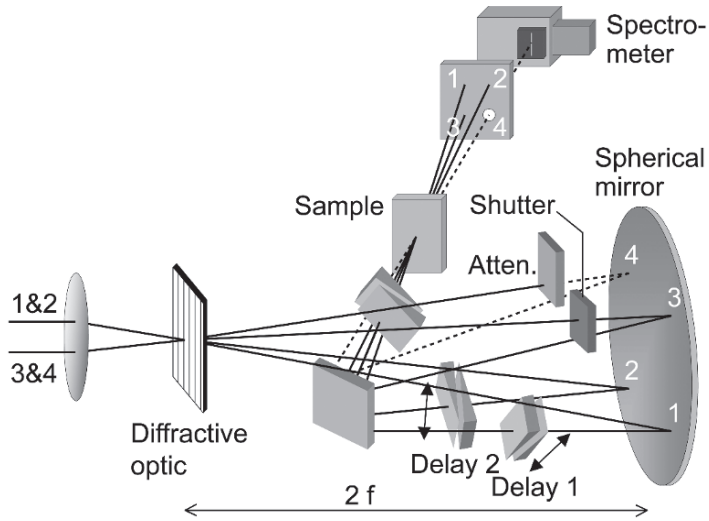

Fig. 9. Inherently phase stabilized 2D spectroscopy setup. The two parallel beams are focused onto the diffractive optic (DO). The first diffraction orders emerge with high efficiency providing all four beams used in the experiments. Beam 4 is the local oscillator. The spherical mirror (2f = 50 cm) creates an image of the pulse overlap in the sample cell via a plane folding mirror. The delays in beam 1 and 2 are provided by computer-controlled movable fused silica wedges. Full characterization of signal field is carried out by spectral interferometry with the attenuated LO. An automated beam shutter is used for subtraction of scattering contributions (Brixner et al., 2004a).

for 2D electronic spectroscopy. The four pulses used in the experiment are arranged in a box geometry (Fig. 9), so that the signal, obeying the phase matching relationship $\mathbf{k}_S = -\mathbf{k}_1 + \mathbf{k}_2 + \mathbf{k}_3$, is emitted in the direction of the fourth local oscillator (LO) pulse $\mathbf{k}_{LO}$. As mentioned above, one major difficulty in electronic 2D spectroscopy is to accomplish phase stability on the timescale of the experiment. To achieve this goal, a diffractive optic (DO) setup (shown in Fig. 9) with passive phase stabilization was built in our laboratory (Brixner et al., 2004a, 2004b). It can be shown that the overall signal phase is stabilized if $-\Delta t_1+\Delta t_2+\Delta t_3-\Delta t_4 = 0$, where Δt_i is a small time shift of the i^{th} beam. This condition is fulfilled in our setup, because the combination of a DO and special geometry compensates for the small timing/phase differences in the four beams introduced by vibrations of the big spherical mirror or folding mirror (for details, see Brixner et al., 2004b). Also, the setup is very compact to guarantee uniform environmental conditions and minimize the effect of any vibrations. The (interferometric) accuracy in the coherence time (τ) delay, which is necessary for Fourier transform spectroscopy, is accomplished by moving fused silica glass wedges with nanometer accuracy in the paths of beams 1 and 2 (Fig. 9). In this way, timing precision of 2.7 as is achieved over the total coherence time scanning range of 400 fs. Complete characterization of the third order signal electric field is obtained by spectral interferometry (Dorrer et al., 2000) of the signal heterodyned (mixed) with the LO. For every population time T, the coherence time τ is typically scanned from −400 to 400 fs by moving pulse 1 from $-(\tau+T)$ to $-T$, and then moving pulse 2 from $-T$ to $-(\tau+T)$ (see Fig. 10). For each population time T and coherence time τ, the total interferometric signal is recorded, given by:

$$I_{SI}(\omega_t) = |E_S(\omega_t)|^2 + |E_{LO}(\omega_t)|^2 + 2\mathrm{Re}E^*_{LO}(\omega_t)E_S(\omega_t)\exp(i\omega_t t_4) \qquad (6)$$

where $E_S(\omega_t)$ is the signal field and $E_{LO}(\omega_t)$ is the local oscillator field for time delay t_4.

The measurement is very sensitive to any scattering signals arriving at the same time as the true photon echo signal. Therefore additional measurements are performed while blocking some of the beams, and background, linear terms and unwanted scattering signals are subtracted. Thus only $S(\omega_t)$, the interference signal between the photon echo and local oscillator corresponding to the third term in Eq. (6), is extracted (Brixner et al., 2004b). The inverse Fourier transform of the interferogram $S(\omega_t)$ is computed in a rotating frame with the central frequency of the spectrum, and a window is applied which keeps only the desired

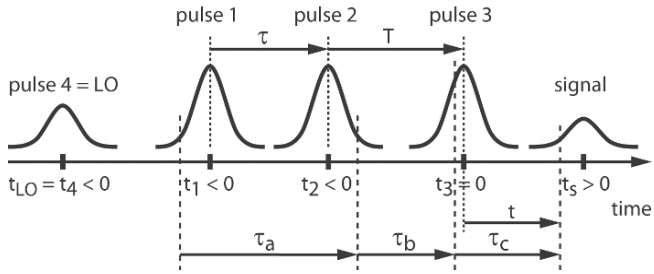

Fig. 10. Pulses and time variables in the heterodyne-detected three photon echo experiment. Time zero is set at the center of the third excitation pulse. The first two excitation pulses are separated by the coherence time τ. The population time T is the separation between the second and third excitation pulses. Nonlinear third order polarization at time t is induced by field interaction at times $\tau_a+\tau_b+\tau_c$, $\tau_b+\tau_c$ and τ_c earlier, which occur under the excitation pulse envelopes. The photon echo signal is observed with an average arrival time t_S that is similar to coherence time. The local oscillator (LO) pulse arrives first at time t_4 (Brixner et al., 2004b).

heterodyne contribution around time t_S-t_4, which is typically 600–800 fs. Here t_S and t_4 are the signal and LO arrival times, correspondingly. After applying the window, a Fourier transform is performed back to the frequency domain and the result is divided by the LO field, obtained in a separate measurement. Thus the complex electric field of the signal for each population and coherence time is equal to

$$E_S(\omega_t) = \frac{F(W(t)F^{-1}S(\omega_t))\exp(-i\omega_t t_4)}{E_{LO}(\omega_t)} \tag{7}$$

where $W(t)$ is a window function. Using Maxwell's equations, it can be seen that the signal electric field in the frequency domain is related to the sample polarization by

$$iP^{(3)}(\tau,T,\omega_t) \sim \frac{n(\omega_t)}{\omega_t} E_S(\tau,T,\omega_t) \tag{8}$$

Here $n(\omega_t)$ is the linear refractive index. Radiative line-shape distortions in the recovered electric field signal are corrected for by multiplication with a factor $n(\omega_t)/\omega_t$. Finally, Fourier transformation along the coherence time τ leads to the 2D spectrum

$$S_{2D}(\omega_\tau,T,\omega_t) = \int_{-\infty}^{\infty} iP^{(3)}(\tau,T,\omega_t)\exp(i\omega_\tau\tau)\,d\tau \tag{9}$$

with two frequency axes corresponding to coherence frequency ω_τ and detection frequency ω_t. However, the 2D spectrum is determined in the relative phase, and therefore the final step of data analysis is obtaining the absolute phase. This is accomplished by determining a constant phase factor following the projection-slice theorem, which states that the real part of the 2D spectrum projected onto the ω_t axis is equal to the spectrally resolved transient electric field spectrum (sometimes called pump-probe, even though it is calculated in a different way than a conventional pump-probe spectrum), which is measured separately (Jonas, 2003).

In order to extract relevant parameters (e.g., electronic couplings between the chromophores) from the 2D spectra, rigorous theoretical simulation of the 2D spectra is necessary. Here we describe just very basic points of the theoretical simulations. For a detailed description see (Brixner et al., 2004b; Cho et al., 2005). Using perturbation theory developed for nonlinear spectroscopy (Mukamel, 1995), the third order polarization in the sample giving rise to the photon echo at time t can be calculated as follows:

$$\begin{aligned} P^{(3)}(t) = \int_0^\infty\int_0^\infty\int_0^\infty & S^{(3)}(\tau_a,\tau_b,\tau_c) \\ & \times E(t-\tau_a-\tau_b-\tau_c)E(t-\tau_b-\tau_c) \\ & \times E(t-\tau_c)d\tau_a d\tau_b d\tau_c \end{aligned} \tag{10}$$

The polarization is induced by the third-order time domain sample response function $S^{(3)}(\tau_a,\tau_b,\tau_c)$ after three electric field interactions with pulses at times $t-\tau_a-\tau_b-\tau_c$, $t-\tau_b-\tau_c$ and $t-\tau_c$ (see Fig. 10 for the ordering of the pulses and time variables). The temporal electric field of laser pulses interacting with the sample is given by

$$E(t) = \tilde{A}(t-t_1)e^{-\omega_0(t-t_1)+i\vec{k}_1\vec{r}} + \tilde{A}(t-t_2)e^{-\omega_0(t-t_2)+i\vec{k}_2\vec{r}}\ \tilde{A}(t-t_3) \times e^{-\omega_0(t-t_3)+i\vec{k}_3\vec{r}} + c.c. \quad (11)$$

with laser carrier frequency ω_0 and complex field amplitude envelopes $\tilde{A}(t)$. Inserting the laser fields of Eq. (11) into Eq. (10) results in 216 terms, however only six terms generate signal in the $-\mathbf{k}_1 + \mathbf{k}_2 + \mathbf{k}_3$ direction along which measurements are performed. The third order response function $S^{(3)}_{rw}(\tau_a,\tau_b,\tau_c)$ is calculated under the rotating-wave approximation (RWA), i.e. the fast oscillating terms, which contribute much less than slowly varying terms after integration, are ignored. The two-dimensional Fourier transformation of $iP^{(3)}_{rw}(\tau,T,t)$ with respect to variables τ and t produces a two-dimensional spectrum for each population time T, which is directly comparable to the 2D spectrum obtained from the experiment.

C. Two-Dimensional Spectroscopy of Light-Harvesting Complexes

Light-harvesting complexes in photosynthesis are multi-chromophoric systems with highly-optimized structures. Information on pigment couplings is crucial for understanding energy transfer pathways resulting in extremely efficient light-harvesting, as well as important quenching mechanisms essential to the survival of photosynthetic organisms under stressful, high-light conditions. 2D electronic spectroscopy was applied to the (FMO) protein complex (Fenna and Matthews, 1975) of green sulfur bacteria *Chlorobium tepidum*, which serves as an antenna and mediator for directing excitations from chlorosome antennae to the reaction center (Brixner et al., 2005; Cho et al., 2005) and to light-harvesting complex III from purple bacteria *Rhodopseudomonas acidophila* (Zigmantas et al., 2006). Herein we discuss the FMO study to illustrate 2D electronic spectroscopy explorations of photosynthetic systems. The FMO complex is a trimer, with each monomer containing seven BChl *a* molecules. Because the inter-complex BChl interactions in the trimer are very weak, only interactions within the monomer were considered. The FMO complex was extensively studied and used as a model system for excitonic interactions because of its relatively simple structure. Approximate coupling constants between BChls, energy levels, and location of excitons in the monomer were estimated in previous experimental and theoretical studies.

Experimental and simulated linear and 2D spectra of FMO are shown in Fig. 11. Note that in order to explore connections between different transitions, the laser spectrum has to cover all transitions of interest in the FMO linear absorption spectrum (Fig. 11d). In 2D spectra, positive features correspond to 'more light', given by stimulated emission and bleaching, and negative features correspond to 'less light', as a result of excited state absorption. Excitonic energy levels are indicated by horizontal and vertical lines. The 2D spectrum of the FMO complex at population time $T = 0$ (Fig. 11a) features diagonal peaks corresponding to linear absorption bands. Elongation of these features indicates inhomogeneous spectral broadening, since it corresponds to the correlation between excitation and emission frequencies within the same pigment. Moreover, analysis of these features can reveal homogeneous linewidths of the corresponding transitions. Most interesting features appear off the diagonal as cross-peaks, e.g., A and B in Fig. 11a. Because of coherent electronic couplings between pigments, nonlinear optical transitions involving two different exciton states are allowed and thus produce cross-peaks already at $T = 0$. Using the assignment of excitonic states, coherent correlations between the excitons can be identified. Cross-peak A indicates that the BChls making up excitons 1 and 5 are coherently coupled, and cross-peak B shows the same for the excitons 2 and 5. Detailed state-to-state energy transfer pathways in the FMO complex can be followed by analyzing the 2D spectra for population times of 200 fs and 1 ps as shown in Fig. 11b, c. It is easily seen that the amplitude of diagonal peak C decreases, and the main diagonal peak D shifts to progressively lower energies at 200 fs and 1 ps as population is transferred downwards. Similarly, downhill transfer is indicated by a concentration of features below the diagonal at detection frequencies ω_t corresponding to the lowest exciton band. Qualitative details of energy transfer pathways can be recognized directly from the spectra. For example, focusing on the two dominant cross-peaks A and B, it is clear that exciton states 4 and 5 relax to exciton state 2 (B) and state 1 (A), skipping state 3. For quantitative information, simulations of the experimental results were performed. A Frenkel exciton Hamiltonian was used with electronic coupling constants and site energies obtained by simultaneously fitting linear absorption and 2D spectra. A single ohmic spectral density and

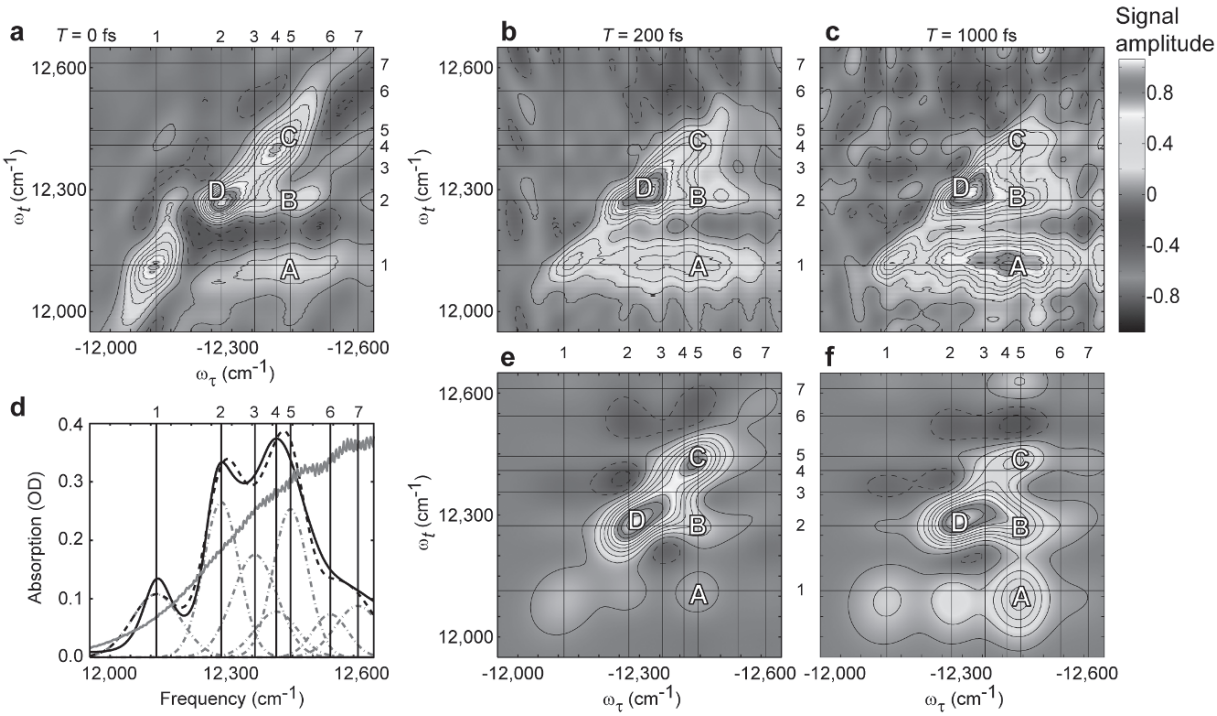

Fig. 11. Experimental and simulated real part of the electric field, corrected for radiative line-shape distortions, of the FMO complex at 77 K. (a-c), The experimental 2D spectra (upper three panels) are shown for population times $T = 0$ fs (a), $T = 200$ fs (b) and $T = 1$ ps (c). Contour lines are drawn in 10% intervals of the peak amplitude, with solid lines representing positive features and dashed lines negative features. Horizontal and vertical grid lines indicate excitonic levels 1−7 as labeled. (d), The experimental (solid black) and simulated (dashed black) linear absorption spectra with individual exciton contributions as shown (dashed-dotted grey). The laser spectrum (solid grey) covers all transition frequencies. (e, f), Simulation of 2D spectra are shown for $T = 200$ fs (e) and $T = 1$ ps (f). Two off-diagonal peaks marked as A and B are indicators of electronic coupling and energy transport, and two diagonal peaks are marked as C and D. (Brixner et al., 2005. Reprinted by permission from Macmillan Publishers Ltd.). See also Fig. 1, Color Plate 6.

modified Förster/Redfield theory were employed for self-consistent calculations of the exciton transfer rates, the linear spectrum, and time-dependent 2D spectra (Fig. 11e, f). Considering the complexity of the system, agreement with the experimental 2D spectra is good. Simulations taking into account the location of different exciton states on different pigments showed that there are two distinct pathways of energy flow after excitation to higher excitonic states. In one pathway, energy from exciton 7 goes directly to exciton 3, then to 2 and finally to the lowest-energy exciton 1. In the second pathway, energy from exciton 6 goes to 5, and then either via 4 or directly to 2, and eventually to 1. Thus the energy is not transferred stepwise down the energy ladder as suggested earlier, but instead follows specific pathways.

2D electronic spectroscopy enables direct determination of the mechanism underlying the evolution of population in complex photosynthetic systems. Furthermore, since 2D electronic spectroscopy is a coherent technique, coherence dynamics on sub-100 fs time can be explored. In summary, the combination of 2D spectroscopy experiments and self-consistent calculations enables the determination of electronic couplings, energy transfer pathways and rates, which depend on spatial distribution of the chromophores in the complex. This leads to the combination of temporal and spatial resolution of complex physical system such as light-harvesting complexes.

VII. Femtosecond Stimulated Raman Spectroscopy

A. Method and Apparatus

Time-resolved Raman spectroscopy has proved to be a very useful tool in tackling dynamic structural

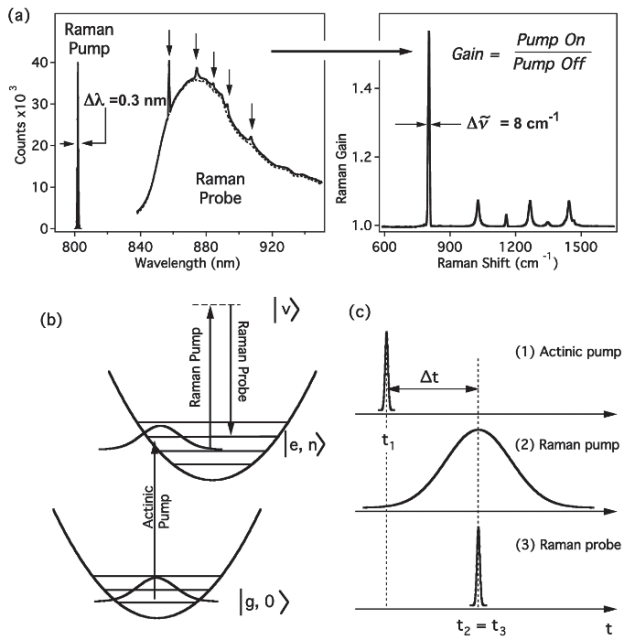

Fig. 12. Illustrative diagrams of the FSRS technique. (a) The spectra of the Raman pump and probe pulses for the experiment on cyclohexane. In the presence of the Raman pump pulse, the stimulated Raman effect amplifies the probe continuum at wavelengths (arrows) shifted by Raman frequencies from the Raman pump wavelength. (b) Energy level diagram showing electronic and vibrational states and vibrational resonances of the three laser pulses. (c) Timing diagram of the FSRS pulses. The Raman pump (2) and Raman probe (3) are optically delayed from the actinic pump (1) by Δt (McCamant et al., 2004). (Fig. courtesy of R.A. Mathies, Univ. of California, Berkeley).

changes in molecules on an ultrafast time scale, as different vibrational modes are very sensitive to molecular conformations and other bond structure changes. Time-resolved Raman techniques were established in the nanosecond regime and subsequently extended to the picosecond regime, but these experiments lacked the time resolution necessary to resolve initial structural changes after excitation, which frequently happen on a fs time scale. Early fs Raman experiments, however, had poor spectral resolution because of the uncertainty principle, which implies that ultrashort duration and narrow spectral bandwidth cannot be combined in a single pulse. The elegant technique of femtosecond stimulated Raman spectroscopy (FSRS) was developed to overcome the problems of time and spectral resolution by introduction of an additional pulse (Yoshizawa and Kurosawa, 2000; Lee et al., 2004; McCamant et al., 2004). In FSRS <100 fs temporal resolution and <10 cm^{-1} spectral resolution can be achieved (McCamant et al., 2004), resulting in an instrument response product of ~1 cm^{-1}ps, which is more than an order of magnitude better than the transform limit of spontaneous Raman (15 cm^{-1} ps).

The scheme of the FSRS technique is shown in Fig. 12. First the molecules in the sample are promoted to an excited electronic state by a resonant actinic pulse of ≤50 fs duration. This pulse can be tuned to match any molecular electronic transition. Then, after a time delay Δt, in order to separate time and spectral resolutions, Raman transitions are probed by two optical fields: the Raman pump at frequency ω_p and the Raman probe at frequency ω_S. The spectral resolution of the experiment is defined by the narrow-bandwidth (3−17 cm^{-1}), picosecond Raman pump pulse at ~800 nm and the inherent spectral resolution of the detection system. The broadband Raman probe pulse is a continuum generated in a sapphire plate or corresponding optical element and compressed to ~30 fs. The spectral region to the red of the Raman pump pulse from 820 nm to 1060 nm can be probed, allowing collection of the full Raman spectrum from 300 to 3050 cm^{-1} (typically a window of 1500 cm^{-1} is used). All three beams (Fig. 12(c)), actinic pump, Raman pump and probe are sent to the sample collinearly, although a crossed geometry may be implemented. The reference beam for shot-to-shot normalization of measured spectra to laser fluctua-

tions is obtained by splitting off part of the Raman probe beam as a reference and measuring it in parallel with the Raman probe beam in the spectrograph. The time resolution is defined by the length of the actinic and Raman probe pulses and the ability to resolve the time delay between the excitation pulse and initiation of the Raman transition by the probe. Stokes frequency lines are probed at frequencies $\omega_{vib}=\omega_p-\omega_S$, and appear in the measurement as sharp spikes in the Raman probe spectrum (Fig. 12(a)). The Raman gain spectrum is calculated by dividing Raman pump-on and pump-off spectra after correcting for the background and fluctuations in the continuum using the reference:

$$Raman\ gain = \frac{[(probe - bkgnd)/(ref - bkgnd)]_{RamanPumpOn}}{[(probe - bkgnd)/(ref - bkgnd)]_{RamanPumpOff}} \quad (12)$$

To obtain excited-state vibrational Raman spectra, contributions from the solvent and electronic ground state vibrational spectra as well as transient absorption of electronic transitions have to be subtracted. Since FSRS measures relatively small changes in the intense Raman probe beam, the technique is fluorescence background free.

B. Time-Resolved Raman Studies of β-Carotene

Understanding the photochemical and photophysical properties of Cars is essential for grasping the crucial role they play in photosynthetic complexes. The femtosecond stimulated Raman technique has been applied to the intensely-studied carotenoid β-carotene (Yoshizawa et al., 2001; McCamant et al., 2003; Kukura et al., 2004). In these experiments β-carotene was excited to the second singlet excited state, S_2 ($1B_u^+$ in C_{2h} symmetry point group notation). The unique combination of spectral and temporal

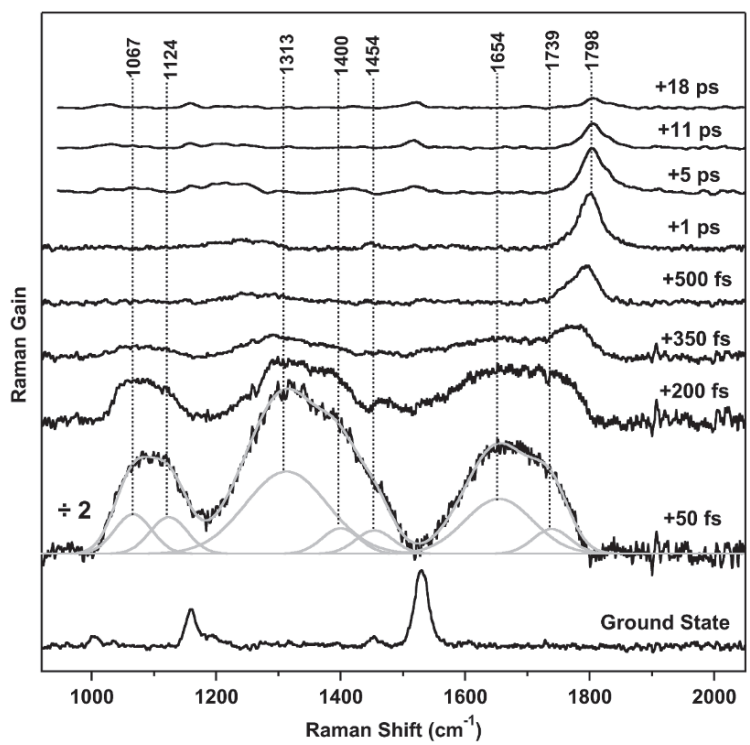

Fig. 13. FSRS spectra of β-carotene in cyclohexane after excitation at 492−497 nm presented as Raman gain versus Raman frequency. Pictured at the bottom is the β-carotene Raman ground state spectrum. The S_2 state Raman spectrum peaks at 50 fs and completely disappears within 500 fs. At the same time, a peak corresponding to the central C=C stretch in the S_1 state appears at 1798 cm^{-1}. A possible decomposition of the signal at 50 fs into Gaussian bands is indicated as grey shapes with corresponding central frequencies (McCamant et al., 2003; Kukura et al., 2004). (Fig. courtesy of R.A. Mathies, Univ. of California, Berkeley).

resolution of FSRS makes it possible to follow relaxation of β-carotene through the manifold of electronic and vibrational states.

FSRS spectra of β-carotene in cyclohexane at selected delay times between the actinic and Raman probe pulses are shown in Fig. 13 (McCamant et al., 2003; Kukura et al., 2004). The ground state β-carotene Raman spectrum is dominated by the methyl rock (C−CH_3) at ~1005 cm^{-1}, the carbon single-bond stretch (C−C) at ~1161 cm^{-1} and the carbon double-bond stretch (C=C) at ~1528 cm^{-1}. The broad features observed for time delays <400 fs are attributed to the second singlet excited state S_2 and decay with time constants of 134 − 161 fs (Kukura et al., 2004). These lifetimes match the β-carotene S_2 state lifetime as measured by transient absorption spectroscopy. At 350 fs, another feature appears on the high-frequency side of the C=C stretch at ~1760 cm^{-1}, which subsequently blue-shifts, narrows, and increases in intensity. It is well known that the C=C stretching frequency in the Car S_1 state is blue-shifted compared to the ground state and appears at 1770 − 1800 cm^{-1}. This shift has been explained in terms of the vibronic coupling between the S_1 and S_2 states through the totally symmetric C=C stretch mode. Thus the peak appearing at ~1760 cm^{-1} was assigned to the C=C vibration in the S_1 state. The evolution of this peak shows rich dynamics as it rises with a ~160 fs lifetime and decays biexponentially with time constants of ~200 fs and 9 ps (McCamant et al., 2003). It also blue-shifts and narrows with a time constant of ~450 fs. The rise of ~160 fs and decay of ~9 ps correspond to S_2−S_1 internal conversion and the lifetime of the S_1 state. The other two sub-fs time constants were attributed to two-step intramolecular vibrational relaxation (IVR), whereby excitation in the C=C mode is first distributed to only the strongly coupled vibrational modes in ~200 fs and then equilibrated throughout the complete set of normal modes in ~450 fs. Note that unlike time resolved absorption, where only overall vibrational relaxation in 400–700 fs was identified, employing FSRS enabled the assignment of two IVR processes to specific vibrational cooling mechanisms.

VIII. Outlook

Over the next ten years, new optical spectroscopy methods will undoubtedly be developed and applied to photosynthetic systems. At the most straightforward, the development of polarization-based multidimensional spectroscopies should be very powerful tools to constrain the products of dipole directions and coupling strengths that determine the strength of cross peaks in two-dimensional spectra of multicomponent complexes (Cho et al., 2005; Cho and Fleming, 2006). Taking a bigger step, perhaps methods will be developed to switch on or off particular interactions in multichromophore complexes, and to measure interactions underlying electron transfer to complement the current advances in understanding of energy transfer (Scholes and Fleming, 2006).

Acknowledgments

This work was supported by the director, Office of Science, Office of Basic Energy Sciences, Chemical Sciences Division of the U.S. Department of Energy under Contract DE-AC03-76SF00098.

References

Aartsma TJ, Louwe RJW and Schellenberg P (1996) Accumulated photon echo measurements of excited state dynamics in pigment-protein complexes. In: Amesz J and Hoff AJ (eds) Biophysical techniques in photosynthesis (Advances in Photosynthesis, Vol 3), pp 109–122. Kluwer Academic Publishers, Dordrecht

Agarwal R, Prall BS, Rizvi AH, Yang M and Fleming GR (2002a) Two-color three pulse photon echo peak shift spectroscopy. J Chem Phys 116: 6243–6252

Agarwal R, Rizvi AH, Prall BS, Olsen JD, Hunter CN and Fleming GR (2002b) Nature of disorder and inter-complex energy transfer in LH2 at room temperature: A three pulse photon echo peak shift study. J Phys Chem A 106: 7573–7578

Asaki MT, Huang CP, Garvey D, Zhou JP, Kapteyn HC and Murnane MM (1993) Generation of 11-fs pulses from a self-mode-locked Ti:sapphire laser. Opt Lett 18: 977–979

Asplund MC, Zanni MT and Hochstrasser RM (2000) Two-dimensional infrared spectroscopy of peptides by phase-controlled femtosecond vibrational photon echoes. Proc Natl Acad Sci USA 97: 8219–8224

Baltuška A, Wei ZY, Pshenichnikov MS and Wiersma DA (1997) Optical pulse compression to 5 fs at a 1-MHz repetition rate. Opt Lett 22: 102–104

Birge RR (1983) One-photon and two-photon excitation spectroscopy. In: Kliger DS (ed) Ultrasensitive Laser Spectroscopy, pp 109–171. Academic Press, New York

Birge RR and Zhang C-F (1990) Two-photon double-resonance spectroscopy of bacteriorhodopsin. Assignment of the electronic and dipolar properties of the low-lying ^1A_g-like and $^1B_u^{*(+)}$-like π,π* states. J Chem Phys 92: 7178–7195

Brixner T, Stiopkin IV and Fleming GR (2004a) Tunable two-dimensional femtosecond spectroscopy. Opt Lett 29: 884–886

Brixner T, Mancal T, Stiopkin IV and Fleming GR (2004b) Phase-stabilized two-dimensional electronic spectroscopy. J Chem Phys 121: 4221–4236

Brixner T, Stenger J, Vaswani HM, Cho M, Blankenship RE and Fleming GR (2005) Two-dimensional spectroscopy of electronic couplings in photosynthesis. Nature 434: 625–628

Butkus R, Danielius R, Dubietis A, Piskarskas A and Stabinis A (2004) Progress in chirped pulse optical parametric amplifiers. Appl Phys B 79: 693–700

Cho MH and Fleming GR (2005) The integrated photon echo and solvation dynamics. II. Peak shifts and two-dimensional photon echo of a coupled chromophore system. J Chem Phys 123: 1–18

Cho MH and Fleming GR (2006) Two-dimensional electronic spectroscopy of molecular complexes. J Chin Chem Soc 53: 15–24

Cho MH, Yu JY, Joo TH, Nagasawa Y, Passino SA and Fleming GR (1996) The integrated photon echo and solvation dynamics. J Phys Chem 100: 11944–11953

Cho MH, Vaswani HM, Brixner T, Stenger J and Fleming GR (2005) Exciton analysis in 2D electronic spectroscopy. J Phys Chem B 109: 10542–10556

De Silvestri S, Nisoli M, Sansone G, Stagira S and Svelto O (2004) Few-cycle pulses by external compression. In: Kärtner FX (ed) Few-Cycle Laser Pulse Generation and its Applications (Topics in Applied Physics, Vol 95), pp 137–177. Springer, Berlin/Heidelberg

deBoeij WP, Pshenichnikov MS and Wiersma DA (1996) System-bath correlation function probed by conventional and time-gated stimulated photon echo. J Phys Chem 100: 11806–11823

Dorrer C, Belabas N, Likforman JP and Joffre M (2000) Spectral resolution and sampling issues in Fourier-transform spectral interferometry. J Opt Soc Am B 17: 1795–1802

Faeder SMG and Jonas DM (1999) Two-dimensional electronic correlation and relaxation spectra: Theory and model calculations. J Phys Chem A 103: 10489–10505

Fenna RE and Matthews BW (1975) Chlorophyll arrangement in a bacteriochlorophyll protein from *Chlorobium-limicola*. Nature 258: 573–577

Fermann ME, Galvanauskas A, Sucha G and Harter D (1997) Fiber-lasers for ultrafast optics. Appl Phys B 65: 259–275

Fischer A, Cremer C and Stelzer EHK (1995) Fluorescence of coumarins and xanthenes after two-photon absorption with a pulsed titanium-sapphire laser. Appl Opt 34: 1989–2003

Friedrich DM and McClain WM (1980) Two-photon molecular electronic spectroscopy. Annu Rev Phys Chem 31: 559–577

Gai F, McDonald JC and Anfinrud PA (1997) Pump-dump-probe spectroscopy of bacteriorhodopsin: Evidence for a near-IR excited state absorbance. J Am Chem Soc 119: 6201–6202

Golonzka O, Khalil M, Demirdoven N and Tokmakoff A (2001) Vibrational anharmonicities revealed by coherent two-dimensional infrared spectroscopy. Phys Rev Lett 86: 2154–2157

Hamm P, Lim MH and Hochstrasser RM (1998) Structure of the amide I band of peptides measured by femtosecond nonlinear-infrared spectroscopy. J Phys Chem B 102: 6123–6138

Hochstrasser RM, Asplund MC, Hamm P and Ge NH (2000) Femtosecond two-dimensional infrared spectroscopy. J Chinese Chem Soc 47: 843–853

Hybl JD, Albrecht AW, Faeder SMG and Jonas DM (1998) Two-dimensional electronic spectroscopy. Chem Phys Lett 297: 307–313

Iaconis C and Walmsley IA (1999) Self-referencing spectral interferometry for measuring ultrashort optical pulses. IEEE J Quantum Elect 35: 501–509

Jimenez R and Fleming GR (1996) Ultrafast spectroscopy of photosynthetic systems. In: Amesz J and Hoff AJ (eds) Biophysical Techniques in Photosynthesis (Advances in Photosynthesis, Vol 3). Kluwer Academic Publishers, Dordrecht

Jimenez R, vanMourik F, Yu JY and Fleming GR (1997) Three-pulse photon echo measurements on LH1 and LH2 complexes of *Rhodobacter sphaeroides*: A nonlinear spectroscopic probe of energy transfer. J Phys Chem B 101: 7350–7359

Jonas DM (2003) Two-dimensional femtosecond spectroscopy. Annu Rev Phys Chem 54: 425–463

Joo TH, Jia YW, Yu JY, Lang MJ and Fleming GR (1996) Third-order nonlinear time domain probes of solvation dynamics. J Chem Phys 104: 6089–6108

Kartner FX, Morgner U, Schibli T, Ell R, Haus HA, Fujimoto JG and Ippen EP (2004) Few-cycle pulses directly from a laser. In: Kärtner FX (ed) Few-Cycle Laser Pulse Generation and its Applications (Topics in Applied Physics, Vol 95), pp 137–177. Springer, Berlin/Heidelberg

Kovalenko SA, Ruthmann J and Ernsting NP (1998) Femtosecond hole-burning spectroscopy with stimulated emission pumping and supercontinuum probing. J Chem Phys 109: 1894–1900

Krueger BP, Yom J, Walla PJ and Fleming GR (1999) Observation of the S_1 state of spheroidene in LH2 by two-photon fluorescence excitation. Chem Phys Lett 310: 57–64

Kukura P, McCamant DW and Mathies RA (2004) Femtosecond time-resolved stimulated Raman spectroscopy of the S_2 ($^1B_u^+$) excited state of beta-carotene. J Phys Chem A 108: 5921–5925

Larsen DS, Papagiannakis E, van Stokkum IHM, Vengris M, Kennis JTM and van Grondelle R (2003) Excited state dynamics of beta-carotene explored with dispersed multi-pulse transient absorption. Chem Phys Lett 381: 733–742

Larsen DS, Vengris M, van Stokkum IHM, van der Horst MA, de Weerd FL, Hellingwerf KJ and van Grondelle R (2004) Photoisomerization and photoionization of the photoactive yellow protein chromophore in solution. Biophys J 86: 2538–2550

Lee SY, Zhang DH, McCamant DW, Kukura P and Mathies RA (2004) Theory of femtosecond stimulated Raman spectroscopy. J Chem Phys 121: 3632–3642

Lide DR (1996) CRC Handbook of Chemistry and Physics. CRC Press, Boca Raton

Linden PA, Zimmermann J, Brixner T, Holt NE, Vaswani HM, Hiller RG and Fleming GR (2004) Transient absorption study of peridinin and peridinin-chlorophyll *a*-protein after two-photon excitation. J Phys Chem B 108: 10340–10345

Logunov SL, Volkov VV, Braun M and El-Sayed MA (2001) The relaxation dynamics of the excited electronic states of retinal in bacteriorhodopsin by two-pump-probe femtosecond studies. Proc Natl Acad Sci USA 98: 8475–8479

Macpherson AN, Arellano JB, Fraser NJ, Cogdell RJ and Gillbro T (2001) Efficient energy transfer from the carotenoid S_2 state in a photosynthetic light-harvesting complex. Biophys J 80: 923–930

McCamant DW, Kukura P and Mathies RA (2003) Femtosecond time-resolved stimulated Raman spectroscopy: Application to the ultrafast internal conversion in β-carotene. J Phys Chem A 107: 8208–8214

McCamant DW, Kukura P, Yoon S and Mathies RA (2004) Femtosecond broadband stimulated Raman spectroscopy: Apparatus

and methods. Rev Sci Instrum 75: 4971–4980
McClain WM (1971) Excited state symmetry assignment through polarized two-photon absorption studies of fluids. J Chem Phys 55: 2789–2796
McClain WM (1974) Two-photon molecular spectroscopy. Acc Chem Res 7: 129–135
McClain WM and Harris RA (1977) Two-photon molecular spectroscopy in liquids and gases. In: Lim EC (ed) Excited states, Vol 3, pp 1–56. Academic Press, New York
Morgner U, Kartner FX, Cho SH, Chen Y, Haus HA, Fujimoto JG, Ippen EP, Scheuer V, Angelow G and Tschudi T (1999) Sub-two-cycle pulses from a Kerr-lens mode-locked Ti:sapphire laser. Opt Lett 24: 411–413
Mukamel S (1995) Principles of Nonlinear Optical Spectroscopy. Oxford University Press, New York
Mukamel S (2000) Multidimensional femtosecond correlation spectroscopies of electronic and vibrational excitations. Annu Rev Phys Chem 51: 691–729
Nisoli M, DeSilvestri S, Svelto O, Szipocs R, Ferencz K, Spielmann C, Sartania S and Krausz F (1997) Compression of high-energy laser pulses below 5 fs. Opt Lett 22: 522–524
Ohta K, Yang M and Fleming GR (2001) Ultrafast exciton dynamics of J-aggregates in room temperature solution studied by third-order nonlinear optical spectroscopy and numerical simulation based on exciton theory. J Chem Phys 115: 7609–7621
Papagiannakis E, Larsen DS, van Stokkum IHM, Vengris M, Hiller RG and van Grondelle R (2004) Resolving the excited state equilibrium of peridinin in solution. Biochemistry 43: 15303–15309
Polivka T and Sundström V (2004) Ultrafast dynamics of carotenoid excited states — from solution to natural and artificial systems. Chem Rev 104: 2021–2071
Prall BS, Parkinson DY, Fleming GR, Yang M and Ishikawa N (2004) Two-dimensional optical spectroscopy: Two-color photon echoes of electronically coupled phthalocyanine dimers. J Chem Phys 120: 2537–2540
Prall BS, Parkinson DY and Fleming GR (2005) Probing correlated spectral motion: Two-color photon echo study of Nile blue. J Chem Phys 123: 054515 (1–13)
Ranka JK, Windeler RS and Stentz AJ (2000) Visible continuum generation in air-silica microstructure optical fibers with anomalous dispersion at 800 nm. Opt Lett 25: 25–27
Ruhman S, Hou BX, Friedman N, Ottolenghi M and Sheves M (2002) Following evolution of bacteriorhodopsin in its reactive excited state via stimulated emission pumping. J Am Chem Soc 124: 8854–8858
Scholes GD and Fleming GR (2006) Energy transfer and photosynthetic light-harvesting. In: Rice SA (ed) Advances in Chemical Physics, Vol 132, pp 57–129. Wiley, New York
Shen YR (1984) The Principles of Nonlinear Optics. John Wiley & Sons, New York
Shima S, Ilagan RP, Gillespie N, Sommer BJ, Hiller RG, Sharples FP, Frank HA and Birge RR (2003) Two-photon and fluorescence spectroscopy and the effect of environment on the photochemical properties of peridinin in solution and in the peridinin-chlorophyll-protein from *Amphidinium carterae*. J Phys Chem A 107: 8052–8066
Spence DE, Kean PN and Sibbett W (1991) 60-fsec pulse generation from a self-mode-locked Ti:sapphire laser. Opt Lett 16: 42–44
Trebino R, DeLong KW, Fittinghoff DN, Sweetser JN, Krumbugel MA, Richman BA and Kane DJ (1997) Measuring ultrashort laser pulses in the time-frequency domain using frequency-resolved optical gating. Rev Sci Instrum 68: 3277–3295
Valkunas L and Gulbinas V (1997) Nonlinear exciton annihilation and local heating effects in photosynthetic antenna systems. Photochem Photobiol 66: 628–634
van Amerongen H, Valkunas L and van Grondelle R (2000) Photosynthetic Excitons. World Scientific, Singapore
Walla PJ, Linden PA, Hsu CP, Scholes GD and Fleming GR (2000) Femtosecond dynamics of the forbidden carotenoid S-1 state in light-harvesting complexes of purple bacteria observed after two-photon excitation. Proc Natl Acad Sci USA 97: 10808–10813
Wilhelm T, Piel J and Riedle E (1997) Sub-20-fs pulses tunable across the visible from a blue-pumped single-pass noncollinear parametric converter. Opt Lett 22: 1494–1496
Xu C and Webb WW (1996) Measurement of two-photon excitation cross sections of molecular fluorophores with data from 690 to 1050 nm. J Opt Soc Am B 13: 481–491
Yan YJ and Mukamel S (1990) Femtosecond pump-probe spectroscopy of polyatomic-molecules in condensed phases. Phys Rev A 41: 6485–6504
Yang M and Fleming GR (1999a) Third-order nonlinear optical response of energy transfer systems. J Chem Phys 111: 27–39
Yang M and Fleming GR (1999b) Two-color three-pulse photon echoes as a probe of electronic coupling in molecular complexes. J Chem Phys 110: 2983–2990
Yang M and Fleming GR (2000) Third-order nonlinear optical response and energy transfer in static disordered systems. J Chem Phys 113: 2823–2840
Yang M, Ohta K and Fleming GR (1999) Three-pulse photon echoes for model reactive systems. J Chem Phys 110: 10243–10252
Yang M, Agarwal R and Fleming GR (2001) The mechanism of energy transfer in the antenna of photosynthetic purple bacteria. J Photochem Photobiol A 142: 107–119
Yoshizawa M and Kurosawa M (2000) Femtosecond time-resolved Raman spectroscopy using stimulated Raman scattering. Phys Rev A 61: 013808 (1–6)
Yoshizawa M, Aoki H and Hashimoto H (2001) Vibrational relaxation of the $^2A_g^-$ excited state in all-trans-β-carotene obtained by femtosecond time-resolved Raman spectroscopy. Phys Rev B 63: 180301 (1–4)
Yu JY, Nagasawa Y, van Grondelle R and Fleming GR (1997) Three pulse echo peak shift measurements on the B820 subunit of LH1 of *Rhodospirillum rubrum*. Chem Phys Lett 280: 404–410
Zigmantas D, Read EL, Mančal T, Brixner T, Gardiner AT, Cogdell RJ and Fleming GR (2006) Two-dimensional electronic spectroscopy of the B800-B820 light-harvesting complex. Proc Natl Acad Sci USA 103: 12672–12677
Zimmermann J, Linden PA, Vaswani HM, Hiller RG and Fleming GR (2002) Two-photon excitation study of peridinin in benzene and in the peridinin chlorophyll a-protein (PCP). J Phys Chem B 106: 9418–9423